Biochemical and Biophysical Research Communications 503 (2018) 2899–2905

Contents lists available at ScienceDirect

Biochemical and Biophysical Research Communications

journal homepage: www.elsevier.com/locate/ybbrc

Crystal structure of the human glial fibrillary acidic protein 1B domain

Bitnarae Kim [a, b], Seungsu Kim [a], Mi Sun Jin [a, *]

[a] School of Life Sciences, GIST, 123 Cheomdan-gwagiro, Buk-gu, Gwangju 61005, Republic of Korea
[b] Advanced Photonics Research Institute, GIST, 123 Cheomdan-gwagiro, Buk-gu, Gwangju 61005, Republic of Korea

ARTICLE INFO

Article history:
Received 6 August 2018
Accepted 7 August 2018
Available online 17 August 2018

Keywords:
Glial fibrillary acidic protein
Intermediate filament
Alexander disease
Rosenthal fibers
Neurodegeneration

ABSTRACT

Glial fibrillary acidic protein (GFAP) is a homopolymeric type III intermediate filament (IF) that plays essential roles in cell migration, mitosis, development, and signaling in astrocytes and a specific type of glial cells. Its overexpression and genetic mutations lead to abnormal IF networks and accumulation of Rosenthal fibers, which results in the fatal neurodegenerative disorder Alexander disease. Herein, we present the first crystal structure of human GFAP spanning the central coiled-coil 1B domain at 2.5 Å resolution. The domain forms a tetramer comprising two equivalent parallel coiled-coil dimers that pack together in an antiparallel manner. Its assembly is stabilized by extensive networks of intermolecular hydrogen bonds, salt bridges, and hydrophobic interactions. Furthermore, mapping of the GFAP mutations associated with Alexander disease reveals that most involve residues buried in the core of the interface, and are likely to disrupt the intermolecular interactions and/or introduce steric clashes, thereby decreasing GFAP solubility and promoting aggregation. Based on our structural analysis and previous biochemical studies, we propose that GFAP assembles in the A11 mode in which coiled-coil 1B dimers lie in close axial proximity in an antiparallel fashion to provide a stable tetrameric platform for the organization of the GFAP filament.

1. Introduction

Intermediate filaments (IFs), together with microtubules and microfilaments, form the cytoskeleton of eukaryotic cells that provides mechanical support and strength to cells and tissues [1]. There are ~70 different genes encoding five classes of IF proteins based on sequence homology and intron position [2]. Glial fibrillary acidic protein (GFAP), along with desmin, peripherin, and vimentin, belongs to the type III IF proteins. Since complete GFAP gene was first identified in mouse [3], a large body of biochemical and physiological evidence indicates that GFAP plays a critical role in cell migration, motility, and mitosis [4]. $GFAP^{-/-}$ mice showed morphological and functional impairment in the blood-brain barrier [5], and displayed loss of white matter and disturbance of myelination in the central nervous system (CNS), indicating a role of GFAP in CNS development [6]. Furthermore, gene expression profiling of GFAP-null astrocytes showed that several genes involved in lysosomal degradation and inflammatory responses are altered, strongly supporting a role for GFAP in cell signaling [7,8].

In the past two decades, more than 200 mutations associated with Alexander disease have been identified throughout the GFAP gene. These mutations lead to abnormal GFAP IF formation and a higher propensity for Rosenthal fibers in astrocytes, which are aggregates of ubiquitinated GFAP proteins along with αB-crystallin and heat shock protein 27 (HSP27) [9]. Overexpression of wild-type GFAP or alteration in its splicing pattern is also found in brain tissues from patients suffering from reactive astrogliosis, including neurotrauma, ischemic stroke, brain tumors, and neurodegenerative disease [9,10]. However, the relevance of these findings for disease mechanisms remains unknown.

All IF proteins typically consist of four α-helical segments (1A, 1B, 2A, and 2B) flanked by non-helical N-terminal head and C-terminal tail domains. The fundamental 'building block' of IFs is an elongated α-helical coiled-coil dimer structure. In general, coiled-coil proteins contain seven-residue heptad repeats, denoted as $(a\text{-}b\text{-}c\text{-}d\text{-}e\text{-}f\text{-}g)_n$, with hydrophobic amino acids leucine, isoleucine, and valine at the *a* and *d* positions, and polar amino acids elsewhere [11]. Residues at the *e* and *g* positions are frequently charged, and influence the orientation and specificity of coiled-coil assembly. Assembly of cytoplasmic IF proteins is initiated by the lateral association of dimers into tetramers, and followed immediately by the formation of nanometer-long unit-length filaments (ULFs).

* Corresponding author.
E-mail address: misunjin@gist.ac.kr (M.S. Jin).

https://doi.org/10.1016/j.bbrc.2018.08.066

ULFs then anneal longitudinally to form short IFs, which ultimately elongate further into a micrometer-long, mature filament [12]. For nuclear lamins, however, elementary coiled-coil dimers start to assemble into polymers via linear head-to-tail association [13].

Crystallization of full-length IF proteins is difficult due to their intrinsic structural flexibility and tendency to self-assemble into filaments. To date, a 'divide-and-conquer' approach is the only method enabling successful structure determination of IF proteins, and this has revealed a central α-helical domain fragmented into short sections of 60–100 residues, the structures of which overlap to establish the complete filament [14]. Using this strategy, structures of several fragments from keratin, vimentin, and lamin have been studied extensively by X-ray crystallography (Table S1). Herein, we present the first crystal structure of the human GFAP 1B domain at 2.5 Å resolution. Structural analysis allows us to understand not only the mechanism of GFAP assembly into filaments, but also its role in Alexander disease at the molecular level.

2. Materials and methods

2.1. Cloning, expression, and purification

The gene encoding the human GFAP 1B domain (residues 110–213) was cloned into the *Nde*I and *Bam*HI sites of the pET15b vector that contains an N-terminal thrombin-cleavable hexahistidine tag. Recombinant protein was produced in *Escherichia coli* BL21 (DE3) cells. Cells were cultured in Luria-Bertani (LB) medium at 37 °C. When the culture reached an absorbance at 600 nm (OD_{600}) of 0.7–0.8, protein expression was induced by addition of 1 mM isopropyl-β-*d*-thiogalactopyranoside (IPTG), the temperature was dropped to 20 °C, and cells were cultured for a further 16 h.

For purification, thawed cells were resuspended in lysis buffer containing 20 mM TRIS-HCl pH 8.0, 200 mM NaCl, 10 mM imidazole, 10 μg/mL DNaseI, and 1 mM phenylmethylsulfonyl fluoride (PMSF). Cells were broken by sonication at 40% amplitude with 30 s on/off pulses for several cycles. Unbroken cells and cell debris were removed by centrifugation at 40,000 g for 20 min, and the supernatant was loaded onto Ni-NTA affinity resin (Incospharm) equilibrated with lysis buffer. Protein was eluted with 20 mM TRIS-HCl pH 8.0, 200 mM NaCl, and 300 mM imidazole. Removal of the histidine tag was achieved by incubating with 0.1% (w/w) thrombin protease for 16 h. The protein was further purified by Superdex 200 (GE Healthcare) gel filtration chromatography.

2.2. Glutaraldehyde crosslinking analysis

For glutaraldehyde-mediated crosslinking, glutaraldehyde (Sigma-Aldrich) was added to purified protein (0.9 mM) at varying final concentrations (2.5%, 0.25%, 0.025%, 0.0025%, and 0.00025% w/v). Mixtures were incubated for 30 min on ice, and reactions were quenched with 20 mM TRIS-HCl pH 8.0, then analyzed on a 15% sodium dodecyl sulfate-polyacrylamide gel electrophoresis (SDS-PAGE) gel.

2.3. Crystallization, data collection, and structure determination

Rod-shaped crystals were grown at 22 °C by the sitting-drop vapor diffusion method using a reservoir solution containing 100 mM TRIS-HCl pH 8.0, 400 mM NaCl, and 22% (w/v) polyethylene glycol (PEG) 10,000. Well-formed crystals were transferred into a cryoprotectant solution containing 100 mM TRIS-HCl pH 8.0, 400 mM NaCl, 27% (w/v) PEG 10,000, and 3% (v/v) EG, and flash-frozen in liquid nitrogen. The diffraction data were processed with the HKL2000 software package (HKL Research Inc.). Initial phases were obtained by molecular replacement (PHASER, CCP4) using the separate helices of the human vimentin 1B structure (PDB code 3UF1) as search models [15]. The atomic model was built using COOT [16]. Refinement of the structure was performed by REFMAC5 [17] and PHENIX [18]. X-ray crystallographic data and refinement statistics are summarized in Table S2. All figures in the manuscript were generated using PyMOL (www.pymol.org).

3. Results and discussion

3.1. The human GFAP 1B domain forms a homotetramer in solution

To explore the oligomeric state of the human GFAP 1B domain (hGFAP_1B) in solution (Fig. 1A), the purified protein was treated with glutaraldehyde and analyzed on SDS-PAGE gels. At low glutaraldehyde concentrations between 0.00025% and 0.025%, monomeric or dimeric forms of hGFAP_1B were evident on gels, whereas at a glutaraldehyde concentration above 0.25%, the major band was shifted to a position corresponding to the tetrameric form of hGFAP_1B, accompanied by the disappearance of the monomer (Fig. 1B). We observed that crosslinked multimeric products of hGFAP_1B migrate more slowly on SDS-PAGE gels than would be expected on the basis of its predicted molecular mass; the dimeric and tetrameric forms of hGFAP_1B were observed at positions corresponding to molecular masses of ~30 and ~60 kDa, compared with calculated molecular masses of 24 and 48 kDa, respectively. Their slower migration during gel electrophoresis is probably due to a significant increase in structural rigidity induced by crosslinking that retards the mobility of multimeric hGFAP_1B through the gel. A shift to the trimeric species was barely observed on SDS-PAGE gels, suggesting that hGFAP_1B is likely to exist as a stable 'dimer-of-dimers' complex.

The oligomeric state of hGFAP_1B in solution was confirmed by size exclusion chromatography. The elution profile revealed the appearance of a single peak between the aldolase (158 kDa) and ovalbumin (43 kDa) protein markers, which corresponds to the molecular weight of the hGFAP_1B tetrameric complex (Fig. 1C). Consistent with the crosslinking data obtained using glutaraldehyde, the hGFAP_1B tetramer displayed a shorter retention time than would be expected for the molecular mass. Taken together, the crosslinking and gel filtration results suggest that the tetrameric assembly of hGFAP_1B provides a structural basis for stability and integrity in the organization of the GFAP filament.

3.2. Overall structure of the human GFAP 1B tetramer

Consistent with the above crosslinking and gel filtration analyses, the crystal structure revealed that hGFAP_1B forms a tetramer comprising two equivalent parallel coiled-coil dimers that pack together in an antiparallel manner (Fig. 2A and S1). The crystallographic asymmetric unit contains two sets of tetramers (Fig. S2) that are fundamentally the same, with Cα root mean square deviation (rmsd) values of 0.3 Å, suggesting that this tetrameric state is structurally stable under our crystallization conditions (Fig. S3). Intriguingly, one half of the hGFAP_1B tetramer exhibits higher B factors than the other half (Fig. S4A). This polarization of structural flexibility appears to be related to the lack of local crystal contacts in the P1 lattice (Fig. S2). Also, formation of the flexible coiled-coil over a large area may allow a more rapid formation of ULFs by regulating precise lateral interactions with other GFAP tetramers.

Given the acidic isoelectric point (pI) of 4.7, we expected that hGFAP_1B would have a strong negative electrostatic potential throughout the protein. However, our structure showed that hGFAP_1B has regions of both negative and neutral charges on the molecular surface (Fig. S4B). This suggests that hydrophobic

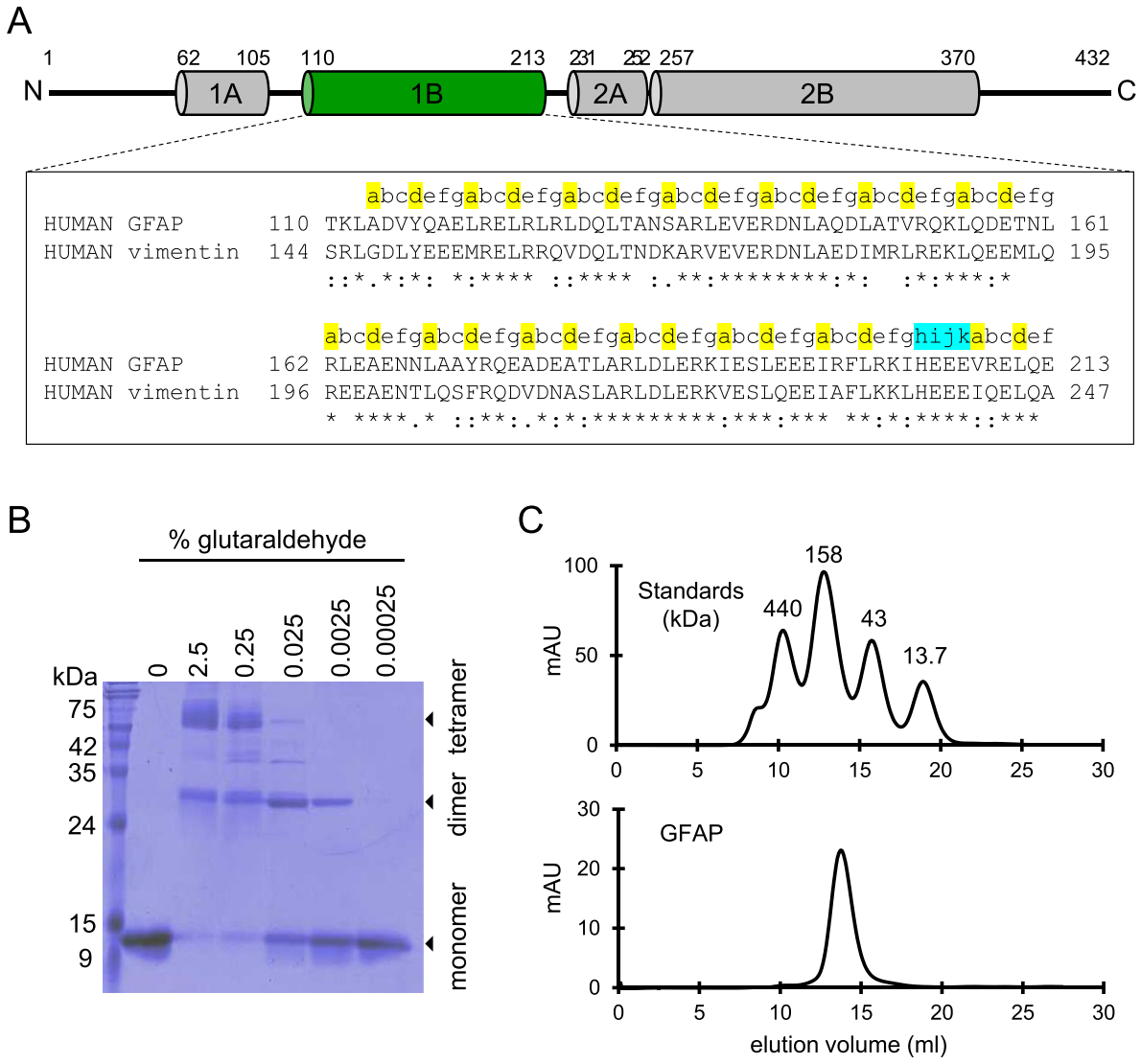

Fig. 1. The GFAP 1B domain forms a homotetramer. (A) Schematic representation of full-length human GFAP. The 1B domain that was crystallized in this study is highlighted in green. Sequence alignment of 1B domains in human GFAP and vimentin is shown underneath the diagram, with the heptad repeat assignment included. Heptad *a* and *d* positions and the 'stutter' region (*h-i-j-k*) are highlighted in yellow and cyan, respectively. (B) Purified hGFAP_1B was crosslinked with various concentrations of glutaraldehyde and analyzed by SDS-PAGE. (C) Size exclusion chromatography profile of purified hGFAP_1B following separation on a Superdex 200 increase 10/300 GL column. Elution of standards is shown in the top panel, and elution of hGFAP_1B is shown in the bottom panel. Molecular mass standards are as follows: thyroglobulin, 669 kDa; ferritin, 440 kDa; aldolase, 158 kDa; ovalbumin, 43 kDa; ribonuclease A, 13.7 kDa.

residues are not only buried in the coiled-coil interface, but also exposed on the solvent-accessible surface, where they can mediate helix-helix interactions and filament organization. This observation is consistent with previous data indicating that a small surface hydrophobic strip composed of four residues in the mouse keratin 16 1B domain plays a critical role in homotetramer stabilization [19]. In our structure, single apostrophes indicate residues that differ between the two large helices.

3.3. Structure of the GFAP 1B coiled-coil dimer

Analysis of the heptad register in hGFAP_1B using the program SOCKET [20] revealed that the homodimeric coiled-coil packing is formed by 13 characteristic heptad repeats (Fig. 1A). The hGFAP_1B dimer interaction is mediated by equivalent hydrophobic residues of the two chains, predominantly leucine, at heptad positions *a* and *d*, following the 'knobs-into-holes' packing arrangement (Fig. 2A and S5) [21]. These homotypic interactions include amino acids A113, L120, L127, L148, L155, L169, A176, I190, I197, and V208 in *a* layers, and Y116, L123, L130, L137, L144, V151, A165, A179, L186, L193, L200, and L211 in *d* layers. The coiled-coil interface of hGFAP_1B also includes charged or polar hydrophobic residues that are relatively unfavorable for the formation of canonical coiled-coils [22]. Aromatic or aliphatic side chains stabilize the hydrophobic core of the coiled-coil, while charged head groups create a number of intermolecular hydrogen bonds (Y116-Q117′, S134-S134′, E158-T159′, and Y172-R173′) and salt bridge (R141-E140′ and E158-R162′) interactions (Fig. 2B–E). This indicates a strong contribution by these residues to dimer stabilization. Interestingly, R183 at the *d* position forms a water-mediated hydrogen bond with the backbone carbonyl oxygen of E178′, allowing the coiled-coil interface to complete the network (Fig. 2F). Notably, hGFAP_1B has two regions lacking this heptad periodicity; the N-terminal three amino acids (110–112), and a 'stutter' region containing four residues (194–197) denoted as *h-i-j-k* at the C-

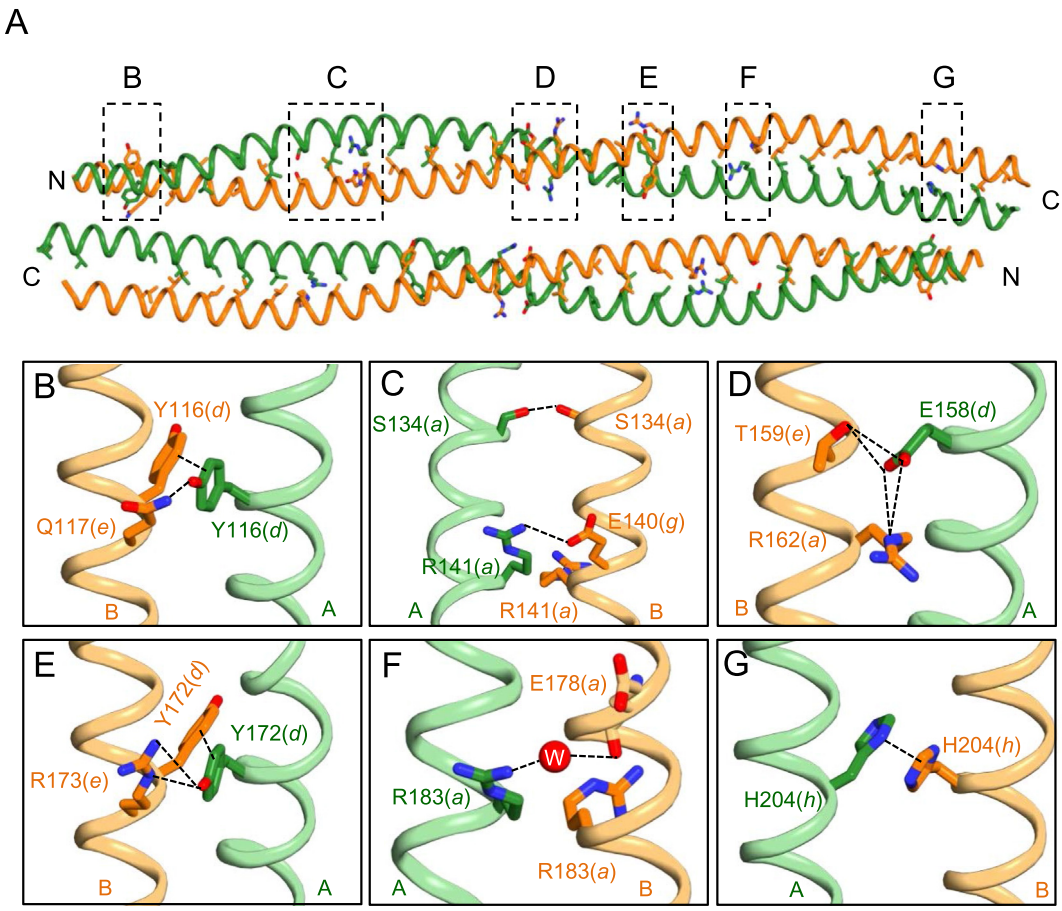

Fig. 2. Structure of the human GFAP 1B domain. (A) The hGFAP_1B tetramer is assembled as a dimer-of-dimers with two parallel α-helices. Residues involved in 'knobs-into-holes' interactions are shown in stick representation. Areas enlarged in (B) to (G) are boxed. (B–G) Detailed dimer interfaces in the hGFAP_1B structure. Residues associated with coiled-coil irregularities are labeled. Heptad repeat positions are written in parentheses. An ordered water molecule (W) is represented by a red sphere.

terminal end [23]. Although these regions were not assigned as heptad repeats, they both adopted an extended α-helix and contributed to the formation of the continuous coiled-coil. In particular, H204 at the *h* position of the stutter region lies within the hydrophobic interface, and plays a key role in maintaining the coiled-coil geometry through π-π stacking interactions via the two imidazole rings (Fig. 2G). These extensive intermolecular interactions in the coiled-coil, together with those in the dimer-dimer interface, may facilitate interaction between hGFAP_1B monomers and stabilize the tetrameric structure (Supplementary Discussion and Figs. S6 and S7).

3.4. Structural comparison between human GFAP and vimentin 1B domains

This study showed that the coiled-coil structure of hGFAP_1B is very similar to that of the corresponding domain of human vimentin, with a Cα rmsd value of 1.7 Å, as expected on the basis of their high sequence identity of 61% (Figs. 1A and 3A). In both structures, the two α-helices (chains A and B) form a highly asymmetric parallel dimer in which chain B has a fully intact α-helix, while chain A is composed of two distinct α-helices. However, superposition analysis revealed small but significant structural differences near the bent region of chain A (residues 169 to 172), where the extent of the bend differs. Calculation using the CCbends program indicated that the coiled-coil axis of hGFAP_1B contains a very large ~15.7° bend in this vicinity (Fig. S8A) [24]. However, vimentin contains a bend of only ~9.2° in the corresponding region. This difference may be associated with two aspects. First, we observed that backbone hydrogen bonds of chain A are broken between residues E166 and A170, as well as N167 and A171, in the hGFAP_1B structure, which presumably increases the flexibility of the molecule at this point (Fig. 3B). By contrast, vimentin contains only one broken hydrogen bond between Q204 and Q208, which correspond to A170 and Q174 in hGFAP_1B, allowing for less flexibility at the vicinity of the bent region (Fig. 3C). Second, we found that two small alanine residues of hGFAP_1B, A176 and A179, are located in the coiled-coil interface, occupying *a* and *d* positions of the heptad repeats (Fig. 3B). As indicated using the program TWISTER [25], these consecutive alanines appear to enable tighter packing of the α-helices by shortening the coiled-coil radius by ~0.8 Å compared with the remaining more canonical segments (Fig. S8B). By contrast, vimentin contains the branched V210 residue, structurally corresponding to A176 of hGFAP_1B, which forms a canonical homotypic core packing interaction with the equivalent residue of the partner helix, indicating increased coiled-coil radius compared with hGFAP_1B (Fig. 3C and S8B). Therefore, the degree of bending is smaller in vimentin than hGFAP_1B. We predict that, despite the high sequence identity, differences in the degree of bending between GFAP and vimentin are likely to affect the specificity of homopolymeric coiled-coil pairing because at least some essential interactions may be missing in the assembly of heteropolymeric coiled-coil dimers.

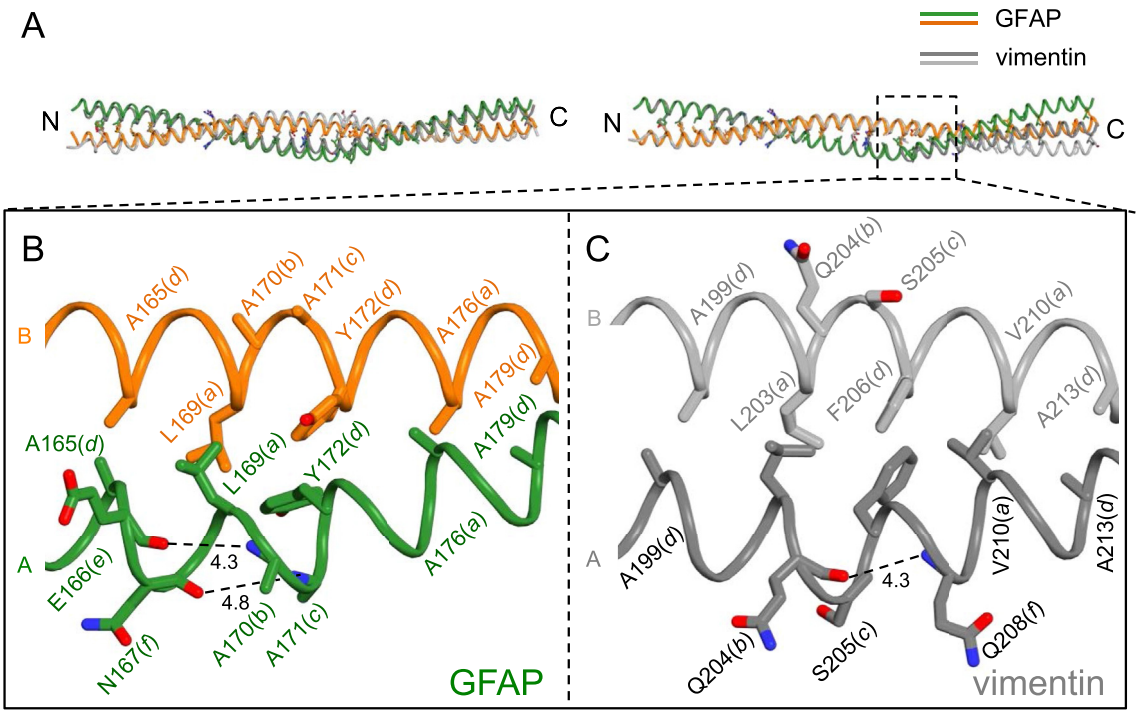

Fig. 3. Comparison of parallel coiled-coil packing in human GFAP and vimentin 1B domains. (A) The coiled-coil 1B domain of human GFAP is pairwise superimposed with that of human vimentin. Least squares alignment of the whole protein (left) and that of the N-terminal half within GFAP (residues 110–160) and the corresponding region of vimentin (residues 144–194, right) are indicated. Chains A and B are drawn as ribbons and colored green and orange in GFAP, and dark and light gray in vimentin, respectively. Areas enlarged in (B) and (C) are boxed. (B) Close-up view of coiled-coil packing in GFAP, and (C) in vimentin, with side chains shown in stick representation.

3.5. Impact of Alexander disease-related mutations on the human GFAP 1B structure

Among Alexander disease-associated mutations identified in GFAP, 14 mutations, including missense, insertion, deletion, and duplication, are present in the rod 1B domain (Table S3). To seek a structural explanation for the impacts of these mutations, we mapped the 14 amino acid changes on the crystal structure of hGFAP_1B determined in this study (Fig. 4A). The results indicate that these alterations may affect the stability of the coiled-coil dimer, as well as the formation of the GFAP tetramer. For example, mutation of V115 to isoleucine or phenylalanine creates steric clashes with the neighboring K202′ and E206′ residues (Fig. 4B) [26], likely resulting in distortion of the helical structure, which would perturb the dimer-dimer interface. In the structure, L123 in heptad position *d* is inserted into a hole formed by the neighboring four residues L120′, L123′, R124, and L127′ in heptad positions *a*, *d*, *e*, and *a*, respectively (Fig. 4C). Accordingly, the L123P mutation may eliminate this characteristic knobs-into-holes interaction, thereby destabilizing the parallel coiled-coil structure [27]. In addition, the L123P mutation results in steric clashes between the proline and the backbone carbonyl oxygens of E119 or L120, which may result in a locally kinked configuration to avoid steric clashes. D128 is involved in key hydrogen bond and ionic interactions with three residues, R188′, K189′, and S192′, in the dimer-dimer interface (Fig. 4D) [28]. Mutation to asparagine may disturb these interfacial interactions due to loss of local negative charge. The structure also indicates that mutation of E207 to valine, glutamine, or lysine would eliminate the stabilizing ionic interaction with H204′ in the coiled-coil interface by altering the local electrostatic potential from negative to positive (Fig. 4E) [26]. In particular, mutations to glutamine or lysine would cause direct collision with H204'. These mutations would likely induce a kink in the helix to avoid charge repulsion or steric clashes, thereby causing aberrant GFAP filament formation. We also mapped D157N, E205K, and E210K mutations on the hGFAP_1B structure (Fig. 4A) [26,28]. The side chains of these residues are not involved in hydrogen bond or electrostatic interactions stabilizing the coiled-coil or tetrameric structure. Rather, they are exposed on the surface of the molecule, and these mutations would change the electrostatic potential at the surface of the molecule without inducing steric clashes. Hence, we predict that these mutations would affect the lateral annealing of GFAP tetramers into ULFs, in turn preventing normal GFAP filament formation.

Compared with the single missense mutations mentioned above, insertion, deletion, and duplication mutations would be expected to cause more severe structural changes in GFAP helices. For example, insertion of amino acids between R124 and L125, or their duplication, may destabilize not only the structure of the α-helix, but also the GFAP tetrameric assembly, due to the loss of ionic interactions with the neighboring E119′ and E196′, and cation-π interactions with F199' (Fig. 4F) [29,30]. Insertion of amino acids between R126 and L127, or their duplication, may result in the loss of hydrophobic interactions with L123′, L127′, and L130' (Fig. 4G) [30,31]. R201 forms a salt bridge interaction with E196′ in the parallel coiled-coil structure; hence its deletion would likely induce local disturbance during coiled-coil assembly (Fig. 4H) [32]. In summary, modeling of Alexander disease-associated mutations based on the hGFAP_1B structure suggests that mutations are likely to destabilize the fundamental helical structure, and result in the loss of stabilizing interactions in the GFAP dimer and tetramer, thereby disrupting *in vivo* GFAP filament assembly.

In summary, we determined the first crystal structure of the human GFAP 1B domain. Similar to the previously reported vimentin structure, our structure suggests that the GFAP filament is assembled via lateral association of two parallel coiled-coil dimers

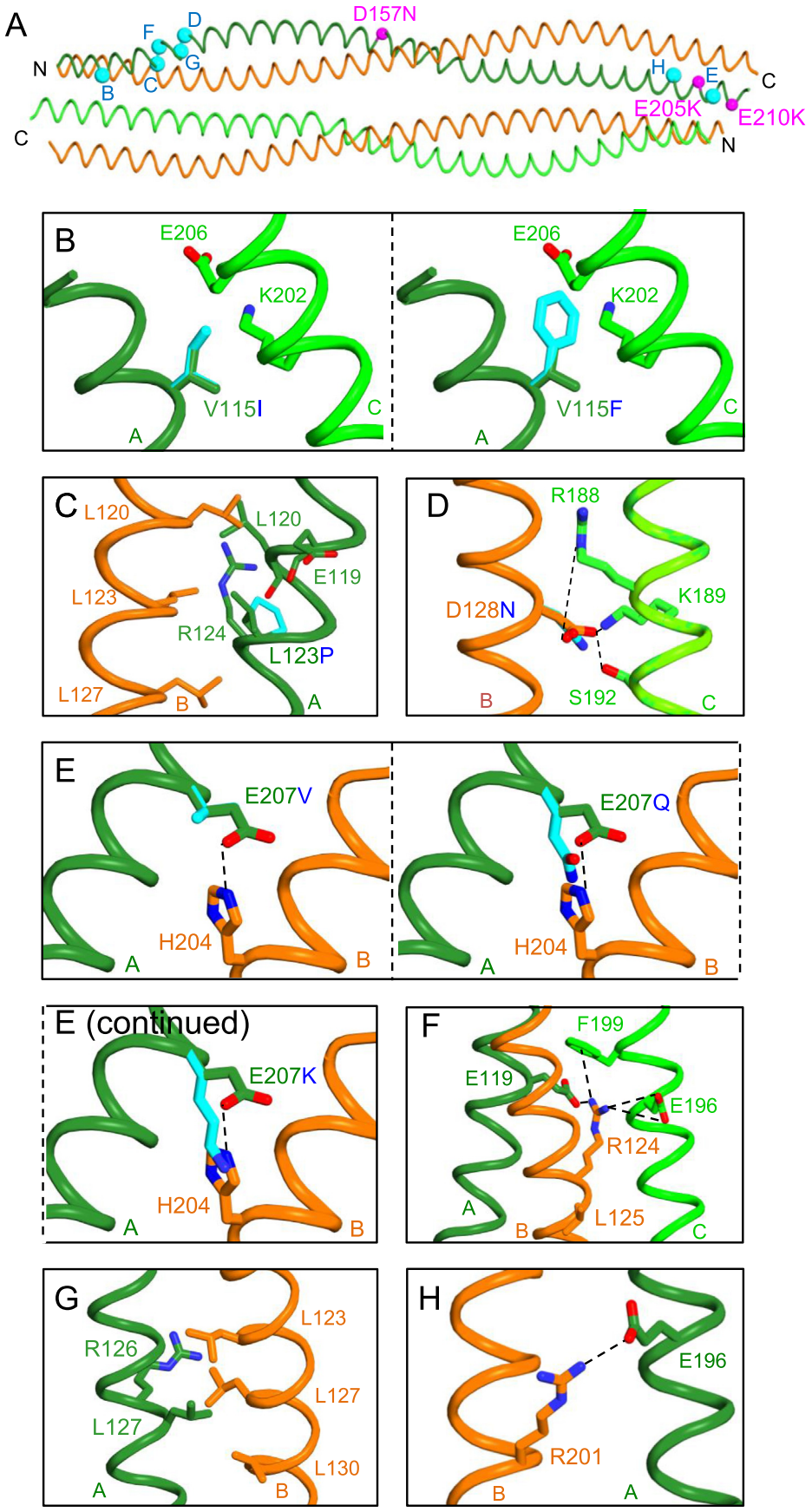

Fig. 4. Structural impacts of Alexander disease-associated mutations on the hGFAP_1B structure. (A) Residues involved in Alexander disease-related mutations are labeled on the hGFAP_1B structure and shown as cyan and magenta balls. (B–H) Close-up views of mutations associated with Alexander disease. The mutated residues are drawn as cyan sticks and superimposed on the corresponding wild-type residues in the hGFAP_1B structure.

with their 1B domains arranged in an antiparallel manner (the A11 mode; Fig. S9). We conclude that extensive networks of intermolecular interactions, together with distinct bending of the helical molecule, increase the stability of the coiled-coil, and the specificity of its intramolecular and intermolecular interactions.

Accession codes

Coordinates and structure factors have been deposited in the Protein Data Bank under accession code 6A9P.

Competing financial interests

The authors declare no competing financial interests.

Acknowledgments

We thank the staff of beamline 7A at the Pohang Accelerator Laboratory (PAL) for assistance during X-ray diffraction data collection. This work was supported by grants from the GIST Research Institute (GRI) funded by GIST in 2018 (grant number GRI_2018).

Transparency document

Transparency document related to this article can be found online at https://doi.org/10.1016/j.bbrc.2018.08.066.

Appendix A. Supplementary data

Supplementary data related to this article can be found at https://doi.org/10.1016/j.bbrc.2018.08.066.

References

[1] E. Fuchs, K. Weber, Intermediate filaments: structure, dynamics, function, and disease, Annu. Rev. Biochem. 63 (1994) 345–382.
[2] P.M. Steinert, A.C. Steven, D.R. Roop, The molecular biology of intermediate filaments, Cell 42 (1985) 411–420.
[3] J.M. Balcarek, N.J. Cowan, Structure of the mouse glial fibrillary acidic protein gene: implications for the evolution of the intermediate filament multigene family, Nucleic Acids Res. 13 (1985) 5527–5543.
[4] E.M. Hol, Y. Capetanaki, Type III intermediate filaments desmin, glial fibrillary acidic protein (GFAP), vimentin, and peripherin, Cold Spring Harb Perspect Biol 9 (2017).
[5] M. Pekny, Astrocytic intermediate filaments: lessons from GFAP and vimentin knock-out mice, Prog. Brain Res. 132 (2001) 23–30.
[6] V. Menet, Y.R.M. Giménez, F. Sandillon, A. Privat, GFAP null astrocytes are a favorable substrate for neuronal survival and neurite growth, Glia 31 (2000) 267–272.
[7] E.M. Hol, M. Pekny, Glial fibrillary acidic protein (GFAP) and the astrocyte intermediate filament system in diseases of the central nervous system, Curr. Opin. Cell Biol. 32 (2015) 121–130.
[8] W. Kamphuis, L. Kooijman, M. Orre, O. Stassen, M. Pekny, E.M. Hol, GFAP and vimentin deficiency alters gene expression in astrocytes and microglia in wild-type mice and changes the transcriptional response of reactive glia in mouse model for Alzheimer's disease, Glia 63 (2015) 1036–1056.
[9] R.A. Quinlan, M. Brenner, J.E. Goldman, A. Messing, GFAP and its role in Alexander disease, Exp. Cell Res. 313 (2007) 2077–2087.
[10] R. Kanski, M.E. van Strien, P. van Tijn, E.M. Hol, A star is born: new insights into the mechanism of astrogenesis, Cell. Mol. Life Sci. 71 (2014) 433–447.
[11] D.A. Parry, Coiled-coils in alpha-helix-containing proteins: analysis of the residue types within the heptad repeat and the use of these data in the prediction of coiled-coils in other proteins, Biosci. Rep. 2 (1982) 1017–1024.
[12] H. Herrmann, M. Häner, M. Brettel, S.A. Muller, K.N. Goldie, B. Fedtke, A. Lustig, W.W. Franke, U. Aebi, Structure and assembly properties of the intermediate filament protein vimentin: the role of its head, rod and tail domains, J. Mol. Biol. 264 (1996) 933–953.
[13] N. Stuurman, S. Heins, U. Aebi, Nuclear lamins: their structure, assembly, and interactions, J. Struct. Biol. 122 (1998) 42–66.
[14] S. Nicolet, H. Herrmann, U. Aebi, S.V. Strelkov, Atomic structure of vimentin coil 2, J. Struct. Biol. 170 (2010) 369–376.
[15] A. Aziz, J.F. Hess, M.S. Budamagunta, J.C. Voss, A.P. Kuzin, Y.J. Huang, R. Xiao, G.T. Montelione, P.G. FitzGerald, J.F. Hunt, The structure of vimentin linker 1 and rod 1B domains characterized by site-directed spin-labeling electron paramagnetic resonance (SDSL-EPR) and X-ray crystallography, J. Biol. Chem. 287 (2012) 28349–28361.
[16] P. Emsley, K. Cowtan, Coot: model-building tools for molecular graphics, Acta Crystallogr D Biol Crystallogr 60 (2004) 2126–2132.
[17] G.N. Murshudov, A.A. Vagin, E.J. Dodson, Refinement of macromolecular structures by the maximum-likelihood method, Acta Crystallogr D Biol Crystallogr 53 (1997) 240–255.
[18] P.D. Adams, P.V. Afonine, G. Bunkóczi, V.B. Chen, I.W. Davis, N. Echols, J.J. Headd, L.W. Hung, G.J. Kapral, R.W. Grosse-Kunstleve, A.J. McCoy, N.W. Moriarty, R. Oeffner, R.J. Read, D.C. Richardson, J.S. Richardson, T.C. Terwilliger, P.H. Zwart, PHENIX: a comprehensive Python-based system for macromolecular structure solution, Acta Crystallogr D Biol Crystallogr 66 (2010) 213–221.
[19] K.M. Bernot, C.H. Lee, P.A. Coulombe, A small surface hydrophobic stripe in the coiled-coil domain of type I keratins mediates tetramer stability, J. Cell Biol. 168 (2005) 965–974.
[20] J. Walshaw, D.N. Woolfson, Socket: a program for identifying and analysing coiled-coil motifs within protein structures, J. Mol. Biol. 307 (2001) 1427–1450.
[21] F. Crick, The packing of α-helices: simple coiled-coils, Acta Crystallogr. 6 (1953) 689–697.
[22] J.M. Mason, K.M. Arndt, Coiled coil domains: stability, specificity, and biological implications, Chembiochem 5 (2004) 170–176.
[23] J.H. Brown, C. Cohen, D.A. Parry, Heptad breaks in alpha-helical coiled coils: stutters and stammers, Proteins 26 (1996) 134–145.
[24] J.H. Brown, How sequence directs bending in tropomyosin and other two-stranded alpha-helical coiled coils, Protein Sci. 19 (2010) 1366–1375.
[25] S.V. Strelkov, H. Herrmann, N. Geisler, T. Wedig, R. Zimbelmann, U. Aebi, P. Burkhard, Conserved segments 1A and 2B of the intermediate filament dimer: their atomic structures and role in filament assembly, EMBO J. 21 (2002) 1255–1266.
[26] R. Li, A.B. Johnson, G. Salomons, J.E. Goldman, S. Naidu, R. Quinlan, B. Cree, S.Z. Ruyle, B. Banwell, M. D'Hooghe, J.R. Siebert, C.M. Rolf, H. Cox, A. Reddy, L.G. Gutiérrez-Solana, A. Collins, R.O. Weller, A. Messing, M.S. van der Knaap, M. Brenner, Glial fibrillary acidic protein mutations in infantile, juvenile, and adult forms of Alexander disease, Ann. Neurol. 57 (2005) 310–326.
[27] P.L. Jany, G.E. Agosta, W.S. Benko, J.C. Eickhoff, S.R. Keller, W. Köehler, D. Koeller, S. Mar, S. Naidu, J. Marie Ness, D. Pareyson, D.L. Renaud, E. Salsano, R. Schiffmann, J. Simon, A. Vanderver, F. Eichler, M.S. van der Knaap, A. Messing, CSF and blood levels of GFAP in alexander disease, eNeuro 2 (2015).
[28] D. Pareyson, R. Fancellu, C. Mariotti, S. Romano, A. Salmaggi, F. Carella, F. Girotti, G. Gattellaro, M.R. Carriero, L. Farina, I. Ceccherini, M. Savoiardo, Adult-onset Alexander disease: a series of eleven unrelated cases with review of the literature, Brain 131 (2008) 2321–2331.
[29] H. Schmidt, B. Kretzschmar, P. Lingor, S. Pauli, P. Schramm, M. Otto, A. Ohlenbusch, K. Brockmann, Acute onset of adult Alexander disease, J. Neurol. Sci. 331 (2013) 152–154.
[30] T. Yoshida, R. Yasuda, I. Mizuta, M. Nakagawa, T. Mizuno, J.A.D.S. Group, Quantitative evaluation of brain stem atrophy using magnetic resonance imaging in adult patients with alexander disease, Eur. Neurol. 77 (2017) 296–302.
[31] M.S. van der Knaap, V. Ramesh, R. Schiffmann, S. Blaser, M. Kyllerman, A. Gholkar, D.W. Ellison, J.P. van der Voorn, S.J. van Dooren, C. Jakobs, F. Barkhof, G.S. Salomons, Alexander disease: ventricular garlands and abnormalities of the medulla and spinal cord, Neurology 66 (2006) 494–498.
[32] S. Varanda, A.F. Santos, T.G. Oliveira, M. Goncalves-Rocha, J. Pereira, J. Fernandes, J. Rocha, Adult onset leukodystrophy-a possible Alexander's disease, Eur. J. Neurol. 22 (2015) 552.